Zeitschrift: Helvetica Physica Acta
Band: 55 (1982)
Heft: 4

Artikel: Single and coincident neutron emission after the absorption of stopped negative pions in 6Li, 7Li, 12C, 59Co and 197Au

Autor: Isaak, H.P. / Heusi, P. / Pruys, H.S.

DOI: https://doi.org/10.5169/seals-115295

Helvetica Physica Acta, Vol. 55 (1982) 477–500 0018–0238/82/040477–24$1.50 + 0.20/0

Single and coincident neutron emission after the absorption of stopped negative pions in ^{6}Li, ^{7}Li, ^{12}C, ^{59}Co and ^{197}Au[1])

By H. P. Isaak, P. Heusi, H. S. Pruys, R. Engfer and E. A. Hermes, Physik-Institut, Universität Zürich, CH-8001 Zürich, Switzerland

and T. Kozlowski[2]), U. Sennhauser[3]) and H. K. Walter, Laboratorium für Hochenergiephysik, ETHZ, CH-5234 Villigen, Switzerland

(1. IX. 1982)

Abstract. Energy spectra of single neutrons, as well as energy spectra and opening angle distributions of coincident neutrons emitted after the absorption of stopped negative pions in ^{6}Li, ^{7}Li, ^{12}C, ^{59}Co and ^{197}Au have been measured. For ^{6}Li 1.55 ± 0.23 and for ^{7}Li 1.73 ± 0.26 highly energetic neutrons ($E_n > 20$ MeV) are emitted per stopped pion. For ^{12}C, ^{59}Co and ^{197}Au the corresponding multiplicities are 1.21 ± 0.18, 1.03 ± 0.15 and 0.90 ± 0.14. The multiplicities of coincident neutrons ($E_{n_1}, E_{n_2} > 20$ MeV) are 0.51 ± 0.09 and 0.61 ± 0.10 $n-n$ events per stopped pion for ^{6}Li and ^{7}Li, and 0.27 ± 0.04, 0.19 ± 0.04 and 0.19 ± 0.04 $n-n$ events per stopped pion for ^{12}C, ^{59}Co and ^{197}Au, respectively. Absorption on an *np* pair, where both nucleons stem from the *p*-shell, leads to the emission of 0.16 ± 0.03, 0.18 ± 0.03 and 0.16 ± 0.03 primary $n-n$ events per stopped pion for ^{6}Li, ^{7}Li and ^{12}C, respectively. Absorption on an *np* pair, where at least one of the two nucleons stems from the *s*-shell, results in 0.28 ± 0.05 and 0.34 ± 0.05 primary $n-n$ events per stopped pion for ^{6}Li and ^{7}Li, respectively. All opening angle distributions are peaked at 180°, the sharpest distribution being that of ^{6}Li. The widths of the opening angle distributions ($E_{n_1}, E_{n_2} > 20$ MeV) are 8.3° and 14.6° HWHM for ^{6}Li and ^{7}Li, and 25°, 40° and 53° HWHM for ^{12}C, ^{59}Co and ^{197}Au, respectively. The widths of the opening angle distributions of primary $n-n$ events steming from *p*-shell absorption are 7.2°, 10.5° and 20.5° HWHM for ^{6}Li, ^{7}Li and ^{12}C. Experimental results are compared with earlier measurements.

1. Introduction

The absorption of stopped negative pions in nuclei starts with the absorption of the pion by two or more correlated nucleons in the nucleus (due to energy and momentum conservation, pion absorption on a single nucleon is strongly supressed). The total energy of the pion (140 MeV) is transferred to the absorbing

---

[1]) Work supported by the Swiss Institute for Nuclear Research (SIN) and the Swiss National Science Foundation.

[2]) On leave from INR, Swierk, Poland.

[3]) Present address, Los Alamos National Laboratory, Group MP-4, MS-846, Los Alamos, New Mexico 87545, U.S.A.

nucleons. These primary nucleons have a high probability of being emitted without any further nuclear interaction. Final-state interactions such as internal scattering, knock-out and pick-up reactions lead to the emission of secondary neutrons and charged particles. The direct particles (primary and secondary ones) are highly energetic and carry away a large part of the available energy. The remaining nucleus is highly excited and de-excites by evaporation of low energetic particles, mainly neutrons, and by the emission of γ-rays. Finally the unstable nucleus decays by β-emission or electron capture.

Experimentally primary, secondary and evaporation particles cannot be separated unambiguously from each other. In very light nuclei, such as ^{6}Li and ^{7}Li, final-state interactions are few, but already in a nucleus such as ^{12}C, these play an important role. The separation of primary from secondary particles requires a model for the pion absorption process [1–6]; evaporation can be distinguished from direct particles by using a standard evaporation model [7].

In the present literature two basic concepts for the primary absorption process are discussed, namely absorption on a pair and on heavier clusters. Most recent theoretical models [1–5] for stopped pion absorption in nuclei consider the absorption of the pion on a pair of nucleons. Yields of residual nuclei [4, 8] and the spectra of neutrons, protons, deuterons and even tritons [2, 4, 5, 9] are explained by this mechanism. Final-state interactions of the primary nucleons with the nucleus strongly contribute or even account completely for the yields of the composite particles. An important parameter in all these calculations is the ratio R of np to pp pairs that can absorb the pion in the nucleus. A comparison of different calculations [2–5] of the spectra of particles emitted after pion absorption shows that R is model dependent. In order to reproduce the experimental proton spectrum, which is most sensitive to the ratio R, values of 2 (Ref. [5]), 3 (Ref. [4]) and even 12 (Ref. [2]) are used for ^{197}Au. The statistical value of R is $R_0 = 2N/(Z-1)$ ($=3$ for ^{197}Au), with N and Z the neutron and proton number. In the calculations of Refs. [4, 5] protons with an energy larger than 20 MeV stem mainly from the primary absorption process on a pp pair, whereas in the calculation of Ref. [2] the proton spectrum up to 80 MeV is dominated by secondary processes. Previous experimental values [10–12] for R are not consistent and usually neither agree with model dependent values, using R as a free parameter [2], nor with values obtained from microscopic calculations [13]. Measurements of single neutron and proton energy spectra [5, 9, 14] yield only lower limits for the ratio R, because of final-state interactions.

Absorption on heavier clusters seems generally to be less important than pair absorption. However, to explain the relatively high yields of deuterons and tritons emitted from very light nuclei such as ^{6}Li and ^{7}Li, a considerable contribution of absorption on heavier clusters must be admitted [14]. A recent calculation [15] of pion absorption rates in ^{12}C shows that at most 10–20% of the measured absorption rate can be explained by mechanisms involving more than two nucleons. The large triton yields found in earlier experiments [12, 16] have often been interpreted as an indication for pion absorption on four nucleons [17]. For ^{12}C an upper limit of 25% four nucleon absorption per stopped pion has recently been estimated from the measured total triton yield [2]. Most recent calculations [2–5], however, postulate final-state interactions to explain the large trition yields, retaining the assumption that the pion is absorbed on an nucleon pair.

Different experimental techniques have been used recently to investigate the

absorption of stopped negative pions in nuclei from ^{3}He to ^{238}U. i] In-beam γ-ray spectroscopy and activation analysis [8] was used to obtain the yields of residual nuclei. ii] Inclusive neutron spectra [9, 18–25], neutron-neutron [10, 11, 21, 26–31], and neutron-charged particle coincidence measurements [6, 10–12, 32] gave information on the pair absorption process, including final-state interactions. iii] inclusive charged particle spectra [14, 16, 25, 33] and charged particle-charged particle coincidence measurements [14] are sensitive tests of cluster absorption mechanisms and final-state interactions. Experimental and theoretical aspects of pion interactions with nuclei have been reviewed by Koltun [34], Kopaleishvilli [35], Hüfner [36], Walter [37] and Buttsev et al. [4].

The present paper gives results from a recent experiment detecting single and coincident neutrons after pion absorption in ^{6}Li, ^{7}Li, ^{12}C, ^{59}Co and ^{197}Au. Single and coincident charged particle data for the same nuclei are published in Ref. [14]. Preliminary results from neutron-charged particle coincidence data, also for the same nuclei, are given in Ref. [6]. For ^{12}C, ^{59}Co and ^{197}Au single and coincidence neutron data already exist [21]. The present coincidence experiment, however, covers a larger angular range and has much better statistics and background conditions. The aim of the present experiment is to have, together with the data of Refs. [6, 14, 21], a consistent set of data for the emission of single and coincident neutrons and charged particles after pion absorption in the nuclei ^{6}Li, ^{7}Li, ^{12}C, ^{59}Co and ^{197}Au. Chapter 2 contains details of the experimental procedure; in Chapter 3 energy spectra of single and coincident neutrons as well as opening angle distributions of two coincident outgoing neutrons are presented and compared with other measurements

2. Experiment and analysis

2.1. *Mechanical set-up and data taking*

The experiments were performed with the vertical $\pi E3$ pion beam line at SIN. Negative pions with a momentum of 82 MeV/c were monitored with a conventional beam telescope, consisting of four plastic scintillators, moderated in polyethylene and brought to rest in targets of about 0.5 g/cm^2 (for ^{6}Li, ^{7}Li, ^{12}C) and 2 g/cm^2 (for ^{59}Co and ^{197}Au). The targets were enclosed in a thin plastic container (0.01 g/cm^2) and positioned at 45° relative to the incident pion beam, which had an average flux of 3 10^6 pions/s for a proton current of 100 μA. The beam telescope rate of pions that stopped in the target was used to normalize the data. Neutrons were detected with 8 liquid organic scintillators (5″ $\varnothing \times 4$″) of type NE 213. The 8 neutron detectors were situated in such a way that $n-n$ coincidence measurements with opening angles θ between 50° and 180° could be performed.[4]) The neutron energy was determined by a time-of-flight (TOF) technique, with a TOF distance of 1.60 m. The time resolution was 1.0 ns FWHM with a neutron detection threshold of 3 MeV. The electronics used in the present

[4]) Although measurements with opening angles of 10°, 20° and 30° were also performed, it was found in the analysis, that at these angles the cross-talk between the two coincident neutron detectors was too large to allow reliable results.

experiment was basically the same as described in Refs. [9, 21]. The anode signals from the neutron detectors and the stopped pion signal from the beam telescope triggered the TOF circuits. The dynode signals of the neutron detectors were used for pulse-shape discrimination of neutrons and gammas and for walk correction of the TOF. Charged particles emitted from the target were vetoed by 1 mm thin plastic scintillator counters in front of the neutron detectors. Threshold calibrations were performed throughout the run with radioactive γ-sources of ^{137}Cs, ^{22}Na, ^{88}Y and AmBe. Time calibrations were also performed regularly and checked with the 50 MHz cyclotron r.f..

2.2 *Data reduction and analysis*

Single and coincident neutron data were treated basically in the same way. The off-line threshold was set to 3 MeV neutron energy. This rather high threshold was choosen for a number of reasons. i] The main interest of the present experiment lies in the high energy region ($E_n > 20$ MeV), where information on the primary absorption process may be obtained. No attempt was made to separate evaporation from direct neutrons. ii] A high threshold reduces the background of neutrons scattered from the floor and surrounding walls. As compared with Refs. [9, 21], no shadow-bar measurements were necessary in the present experiment. iii] Corrections for walk in timing were small and the separation of neutrons from gammas was very good. iv] Neutron efficiency calculations tend to be more reliable for higher thresholds.

The measured TOF was corrected for walk in timing as a function of the pulse height of the dynode signals. For neutron energies above 3 MeV, the walk correction was less than 0.4 ns. In the off-line analysis, neutrons and gammas were distinguished by comparing the fast and slow parts of the dynode signals. The contamination of gammas in the neutron spectra was less than 4%. The neutron TOF was transformed to neutron energy using relativistic kinematics. The neutron energy spectra were corrected for neutron detection efficiency and were absolutely normalized after background subtraction. The neutron detection efficiency was calculated with a Monte Carlo program developed at Saclay (see Chapter 2.3.). The background of neutrons correlated to pion stops in the third counter of the beam telescope and in the plastic container was determined from a measurement with the target removed. The background spectrum was identical with the spectrum of neutrons emitted after pion absorption in ^{12}C. A flat accidental background of neutrons was also subtracted. It was of minor importance and was determined by neutrons with negative TOF. Fig. 1 shows a measured TOF spectrum of neutrons emitted after pion absorption in ^{6}Li and the corresponding background spectrum. The fact that the accidental background for negative TOF is only slightly lower than the accidental background of neutrons below the threshold shows that there is hardly any background from scattered neutrons. Coincidence spectra were basically treated in the same way as single spectra except that instead of one dimensional energy spectra, two dimensional energy spectra were produced. The coincidence spectra were further corrected for the semi-accidental background i.e. neutrons correlated with a stopped pion and detected in coincidence with an accidental neutron. This background was much larger than the true accidental background (determined from events with negative

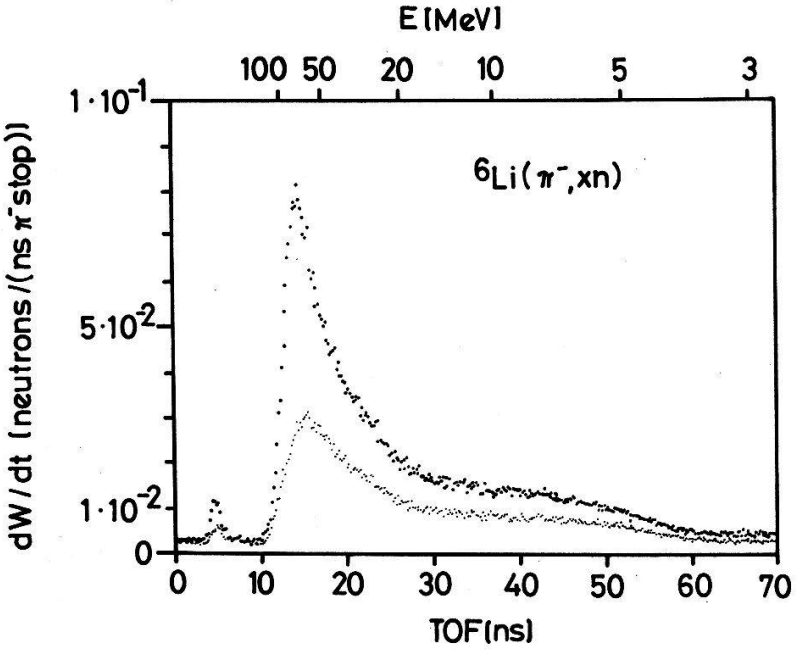

Figure 1
TOF spectrum of neutrons emitted after the absorption of stopped negative pions in ^{6}Li (large points) and the corresponding background spectrum without target (small points). The spectra are normalized to the number of stopped pions, but are not corrected for neutron detection efficiency. Due to imperfect $n-\gamma$ discrimination, a small gamma peak can be seen in the measured neutron spectra.

TOF for both detectors) and was determined from events with a negative TOF for one and a positive TOF for the other detector. Whereas the true accidental background is flat, the projection of the semi-accidental background on one axis has the spectral shape of a single spectrum. Both the energy spectra of neutrons with and without target were treated in the same way. The normalized single and coincident neutron energy spectra were determined as follows:

$$\frac{dW}{dE_n} = \frac{4\pi}{\Omega_{sr}} \cdot \frac{T-B}{\varepsilon S} \qquad \text{[single } n\text{]}$$

$$\frac{d^3W}{dE_{n_1}\, dE_{n_2}\, d\cos\theta} = \frac{8\pi^2}{\Omega_{sr}^2} \cdot \frac{T-B}{2\varepsilon_1\varepsilon_2 S} \qquad \text{[coincidence } n-n\text{]}$$

where θ is the opening angle of the two coincident neutrons, ε the neutron detection efficiency, S the number of true pion stops in the target, and T and B the measured neutron energy spectra with and without target, respectively. The factor 2 comes from the fact that the neutrons are indistinguishable. The solid angle of one neutron detector was $\Omega_{sr} = 4.95\ 10^{-3}$ sr. All beam telescope rates were corrected for computer dead time and pile-up. In the single neutron measurements about 10^9 pions were stopped in each target; in the coincidence $n-n$ measurements 10^{11} pions were stopped in ^{6}Li, ^{7}Li and ^{12}C and about 10^{10} pions in ^{59}Co and ^{197}Au.

2.3. *Neutron detection efficiency*

The three most recently measured spectra of neutrons emitted after pion absorption in ^{12}C [21–23] differ only slightly in spectral shape. This can partly be attributed to the different determinations of the neutron detection efficiency.

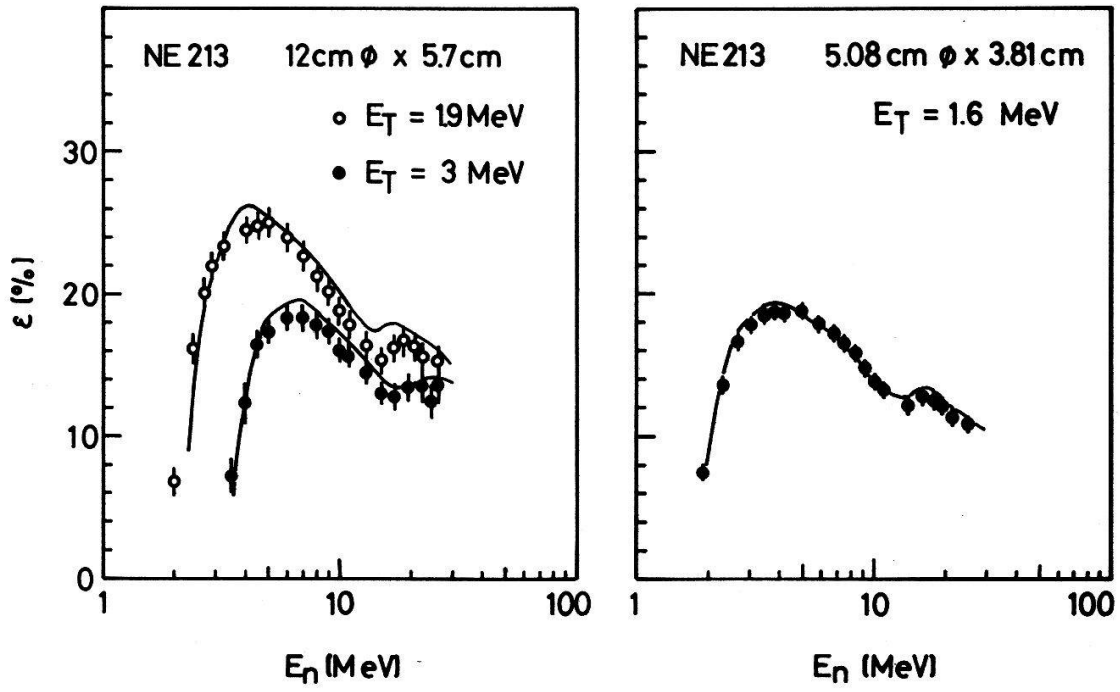

Figure 2
Comparison of the present efficiency calculations (solid lines) with measurements for NE 213 (Ref. [42]: 12 cm ∅ × 5.7 cm and neutron energy threshold $E_t = 1.9$ and 3 MeV; Ref. [43]: 5.08 cm ∅ × 3.81 cm and $E_t = 1.6$ MeV).

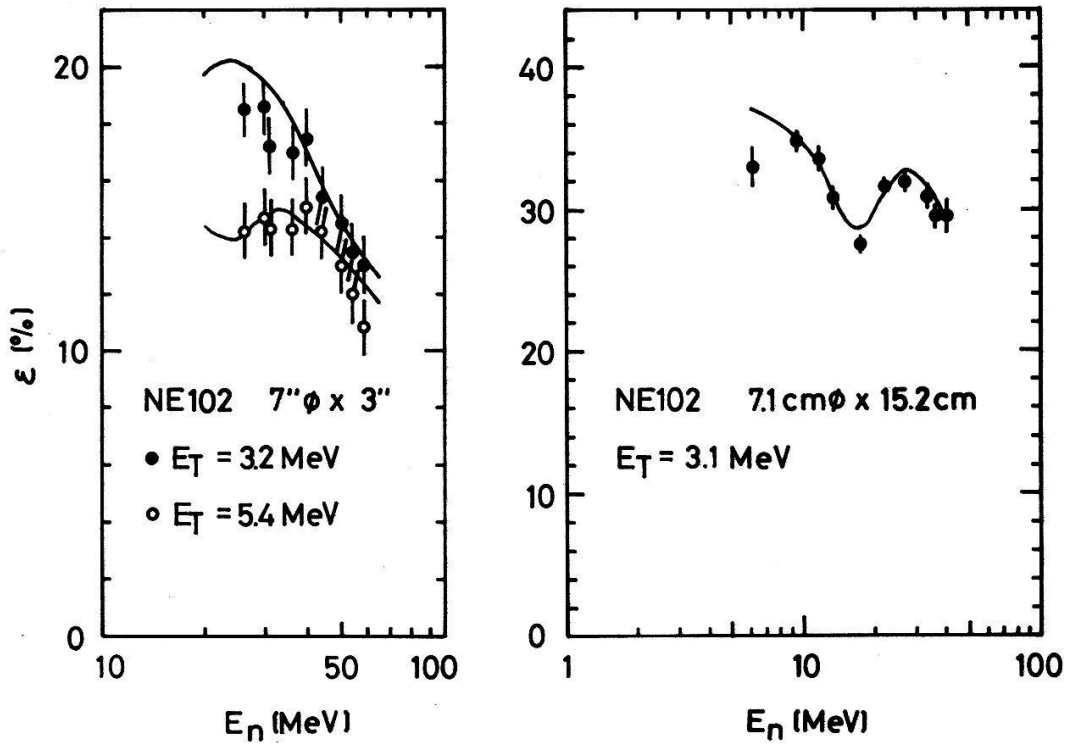

Figure 3
Comparison of the present efficiency calculations (solid lines) with measurements for NE 102 (Ref. [44]: 7″ ∅ × 3″ and $E_t = 3.2$ and 5.4 MeV; Ref. [45]: 7.1 cm ∅ × 15.2 cm and $E_t = 3.1$ MeV).

Hartmann et al. [21] used the Oak Ridge computer code 05-S, Klein et al. [22] the Stanton code [38] and Madey et al. [23] the code of Cecil et al. [39], which is an improved version of the Stanton code. Both the Oak Ridge and original Stanton codes use an earlier set of data for the various neutron-induced cross sections. The present Monte Carlo code is based on the code of Del Guerra et al. [40] and was updated by Vernin [41].

To test the reliability of the present calculations, comparisons were made with different experimental data for detectors of type NE 213 and NE 102. In Fig. 2 the calculations are compared with the data of Drosg [42] (12 cm ∅ × 5.7 cm and neutron energy threshold $E_t = 1.9$ and 3 MeV) and Fowler et al. [43] (5.08 cm ∅ × 3.81 cm and $E_t = 1.6$ MeV) for NE 213. The overall agreement is good over the entire energy range of the measurements. In general, the present calculations overestimate the measurements of Ref. [42] by 5 to 10%, with a maximum discrepancy of 15% in the region between 14 and 18 MeV for a 1.9 MeV threshold. For a 3 MeV threshold at energies above 18 MeV the agreement is good. The data of Ref. [43] agree very well with the calculations. The measurements for NE 213, however, extend only up to energies around 25 MeV. Therefore, a further comparison is made in Fig. 3 with the data of Riddle et al. [44] (7″ ∅ × 3″ and $E_t = 3.2$ MeV and 5.4 MeV) and McNaughton et al. [45] (7.1 cm ∅ × 15.2 cm and $E_t = 3.1$ MeV) for NE 102, where measurements exist for energies up to 66 MeV. The agreement with the data of Ref. [44] is quite good. With reference to Anghinolfi et al. [46], the efficiency for a 3.2 MeV neutron threshold were shifted by 0.02, assuming that there was an error in the lettering of Fig. 3 of Ref. [44]. The agreement of the calculations with the measurement of Ref. [45] is good for energies higher than 10 MeV. The efficiency used in the present work is depicted in Fig. 4 (5″ ∅ × 4″ and $E_t = 3$ MeV). Fig. 5 compares the present code with the Oak Ridge code (used for the neutron measurements of

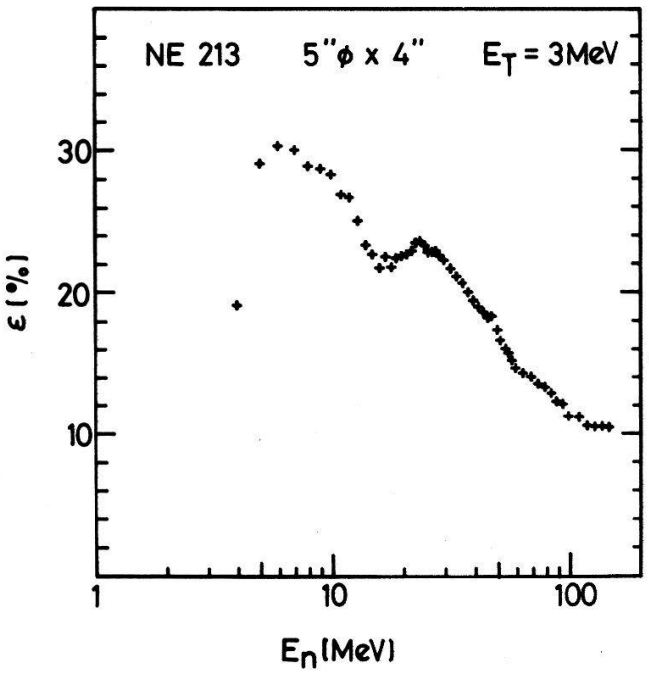

Figure 4
Present neutron detection efficiency ε for a 5″ diameter and 4″ thick neutron detector of type NE 213 for a neutron energy threshold of $E_t = 3$ MeV (equivalent to an electron energy $E_e = 973$ keV).

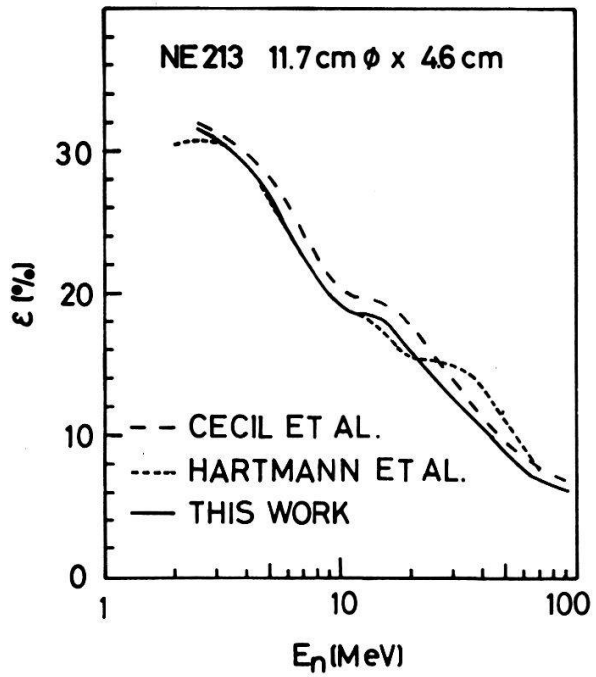

Figure 5
Comparison of the present efficiency calculations with other calculations for NE 213 (Oak Ridge code of Hartmann et al. [21] and the code of Cecil et al. [23, 39]: 11.7 cm ∅ × 4.6 cm and $E_t = 1$ MeV).

Ref. [21]) and the code of Cecil et al. [39] (used for the neutron measurements of Ref. [23]). The calculations were made for the detector of Ref. [21] (11.7 cm ∅ × 4.6 cm and $E_t = 1$ MeV). The present calculations differ from the Oak Ridge calculations mainly in the energy region from 20 to 50 MeV. The calculations of Cecil et al. [39] agree very well in shape with the present calculations, but are somewhat higher in absolute magnitude.

3. Results and discussion

3.1. *Single neutron spectra*

The energy spectra of neutrons emitted after the absorption of stopped negative pions are shown in Fig. 6 for ^{6}Li and ^{7}Li and in Fig. 7 for ^{12}C, ^{59}Co and ^{197}Au. Measured neutron multiplicities are given in Table 1. The low energy parts of the spectra ($E_n < 10$ MeV) are dominated by evaporation[5]) and for the very light nuclei also by secondary neutrons. The multiplicities of neutrons emitted with energies between 3 and 10 MeV increase with increasing mass number A and are 0.31 ± 0.05, 0.89 ± 0.13 and 1.56 ± 0.23 neutrons per stopped pion for ^{12}C, ^{59}Co and ^{197}Au. The corresponding numbers for ^{6}Li and ^{7}Li are 0.34 ± 0.05

[5]) In the present paper, evaporation and non-evaporation neutrons were not separated by means of an evaporation formula. For ^{12}C, ^{59}Co and ^{197}Au this has been done in Ref. [21] and for ^{6}Li and ^{7}Li an evaporation fit is anyhow problematic. Ni isotopes and a number of heavy nuclei from ^{165}Ho to ^{238}U have been measured in Ref. [9], where this separation has been discussed in detail.

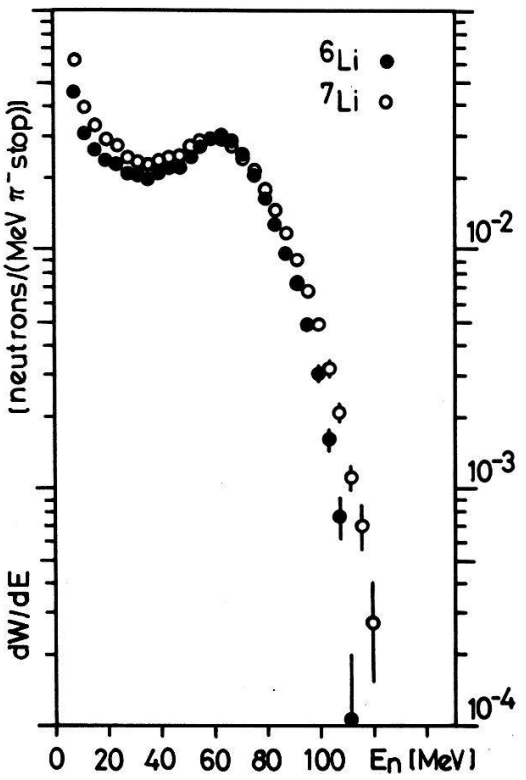

Figure 6
Energy spectra of neutrons ($E_n > 5$ MeV) emitted after the absorption of stopped negative pions in ^{6}Li and ^{7}Li. The errors shown are statistical only, the error in normalization is 15%. The error in energy is 2.4% at 5 MeV, 3.2% at 10 MeV, 4.4% at 20 MeV, 6.9% at 50 MeV and 10% at 100 MeV.

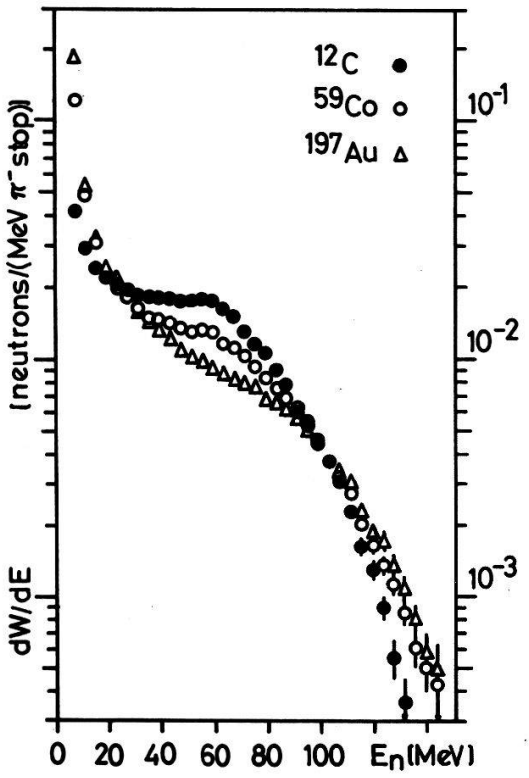

Figure 7
Energy spectra of neutrons ($E_n > 5$ MeV) emitted after the absorption of stopped negative pions in ^{12}C, ^{59}Co and ^{197}Au.

Table 1
Measured multiplicities X_m of neutrons emitted per stopped pion after the absorption of stopped negative pions in ^{6}Li, ^{7}Li, ^{12}C, ^{59}Co and ^{197}Au are compared with other results. Multiplicities are tabulated for different energy thresholds (E_t is the off-line detection threshold of the measurement).

Target	E_t	X_m $E_n > E_t$	X_m $E_n > 5$ MeV	X_m $E_n > 10$ MeV	X_m $E_n > 20$ MeV	X_m $E_n > 40$ MeV	References
^{6}Li	3 MeV	2.15(32)	2.02(30)	1.81(27)	1.55(23)	1.13(17)	This work
	2.5 MeV	2.34(32)	2.20(30)[a]				Ref. [20]
^{7}Li	3 MeV	2.52(38)	2.35(35)	2.06(31)	1.73(26)	1.24(19)	This work
	2.5 MeV	2.52(32)	2.34(30)[a]				Ref. [20]
^{12}C	3 MeV	1.77(27)	1.66(25)	1.46(22)	1.21(18)	0.83(12)	This work
	1.2 MeV	2.26(17)	1.83(14)	1.60(12)	1.29(10)	0.86(6)	Ref. [23]
	3 MeV	2.05(25)	1.86(22)				Ref. [22][a]
	2 MeV	1.89(15)	1.64(13)	1.45(12)	1.21(12)	0.86(7)	Ref. [21]
	2.5 MeV	2.73(34)	2.52(31)[a]				Ref. [20]
	1.8 MeV	2.8(3)	2.6(3)[a]				Ref. [19]
^{59}Co	3 MeV	2.25(34)	1.91(29)	1.36(20)	1.03(15)	0.69(10)	This work
	2 MeV	3.10(18)	2.07(12)	1.49(9)	1.06(6)	0.72(4)	Ref. [21]
^{62}Ni	1.2 MeV	3.9(8)	1.9(3)	1.2(2)	0.8(2)	0.5(1)	Ref. [9]
^{nat}Cu	1.2 MeV	4.02(55)	2.11(30)	1.45(20)	1.11(15)	0.71(11)	Ref. [23]
	2.5 MeV	4.02(50)	3.25(40)[a]				Ref. [20]
	3 MeV	4.7(3)	3.5(2)				Ref. [18][a]
^{197}Au	3 MeV	2.82(42)	2.08(31)	1.26(19)	0.90(14)	0.56(8)	This work
	1.2 MeV	4.5(7)	1.8(3)	1.2(2)	0.89(14)	0.5(1)	Ref. [9]
	2 MeV	3.70(22)	1.81(11)	1.25(8)	0.94(6)	0.61(4)	Ref. [21]
^{nat}Pb	1.2 MeV	5.87(141)	2.06(50)	1.46(35)	1.10(26)	0.67(16)	Ref. [23]
	1.2 MeV	4.5(7)	1.7(3)	1.3(2)	0.93(14)	0.6(1)	Ref. [9]
	2.5 MeV	3.74(44)	2.70(31)[a]				Ref. [20]
	1.8 MeV	3.5(4)	2.2(3)[a]				Ref. [19]
	3 MeV	6.7(4)	5.2(3)				Ref. [18][a]

[a] In Refs. [18, 22] only total multiplicities for all neutrons with $E_n > 0$ MeV (including extrapolated evaporation neutrons below the threshold) are given. In Refs. [19, 20] measured multiplicities are given only for $E_n > 1.8$ and 2.5 MeV, respectively. In order to allow a comparison with the other data the multiplicities for $E_n > 3$ and/or 5 MeV have been extracted from the total multiplicities of Refs. [18–20, 22] by subtracting the evaporation multiplicities for $E_n < 3$ and/or 5 MeV, respectively (the evaporation multiplicities were obtained by integrating the LeCouteur formula [7]).

and 0.46 ± 0.07, respectively. The intermediate energy parts of the spectra ($10 < E_n < 20$ MeV) are determined largely by secondary processes. The multiplicities of neutrons emitted with energies in this region are the same for all measured targets, namely about 0.31 ± 0.05 neutrons per stopped pion. The high energy parts of the spectra ($E_n > 20$ MeV) stem largely from the primary absorption process. For ^{6}Li 1.55 ± 0.23 and for ^{7}Li 1.73 ± 0.26 highly energetic neutrons are emitted per stopped pion. The corresponding multiplicities for ^{12}C, ^{59}Co and ^{197}Au decrease with increasing mass number A and are 1.21 ± 0.18, 1.03 ± 0.15 and 0.90 ± 0.14 neutrons per stopped pion, respectively. The characteristic high energy enhancement ($E_n \sim 60$ MeV) clearly seen in the neutron energy spectra of ^{6}Li and ^{7}Li, and somewhat in ^{12}C, is a signature of the primary absorption process on an *np* pair. This enhancement becomes even more prominent in the $n-n$ coincident measurements (see Chapter 3.2.).

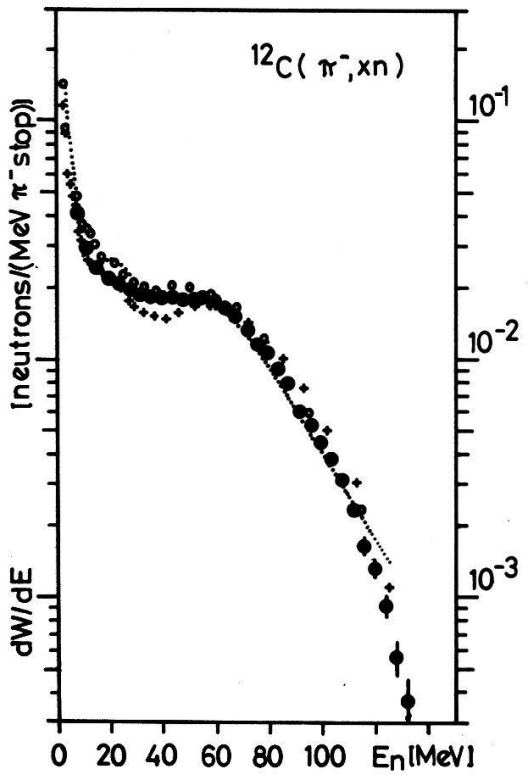

Figure 8
The present (large full circles) energy spectrum of neutrons emitted after the absorption of stopped negative pions in ^{12}C is compared with the measurements of Ref. [21] (crosses), Ref. [22] (dotted line) and Ref. [23] (small open circles).

In Table 1 the measured neutron multiplicities are compared with results from other measurements [9, 18–23]. The agreement with older measurements [18–20] is generally better for the light nuclei (^{6}Li, ^{7}Li and ^{12}C) than for the medium and heavy nuclei (^{59}Co and ^{197}Au), where results differ by even a factor of 2. The agreement with newer measurements [9, 21–23] is generally good. In Fig. 8 the energy spectrum of neutrons emitted after pion absorption in ^{12}C is compared with the measurements of Hartmann et al. [21], Klein et al. [22] and Madey et al. [23]. The only difference between the present ^{12}C data and that of Ref. [21] lies in the region from 30 to 50 MeV and is due to a difference in efficiency (see Fig. 5). The small differences in the spectral shape of the other measurements also come mainly from the different efficiency codes used and are discussed in detail in Ref. [23], where the data of Refs. [21, 22] were reanalyzed using common efficiency calculations. The remaining slight discrepancies could result from differences in the background subtracted.

3.2. *Coincident neutron spectra*

3.2.1 *Results for* ^{6}Li *and* ^{7}Li. Two dimensional neutron-neutron energy spectra and neutron-neutron opening angle distributions were measured for pion absorption in ^{6}Li and ^{7}Li for opening angles θ from 50° to 180°.[6]) Fig. 9 shows the

[6]) The measurements using two diametrical neutron detectors will be referred to as the 180° measurement, although the mean opening angle θ for this geometry is actually 177.5°.

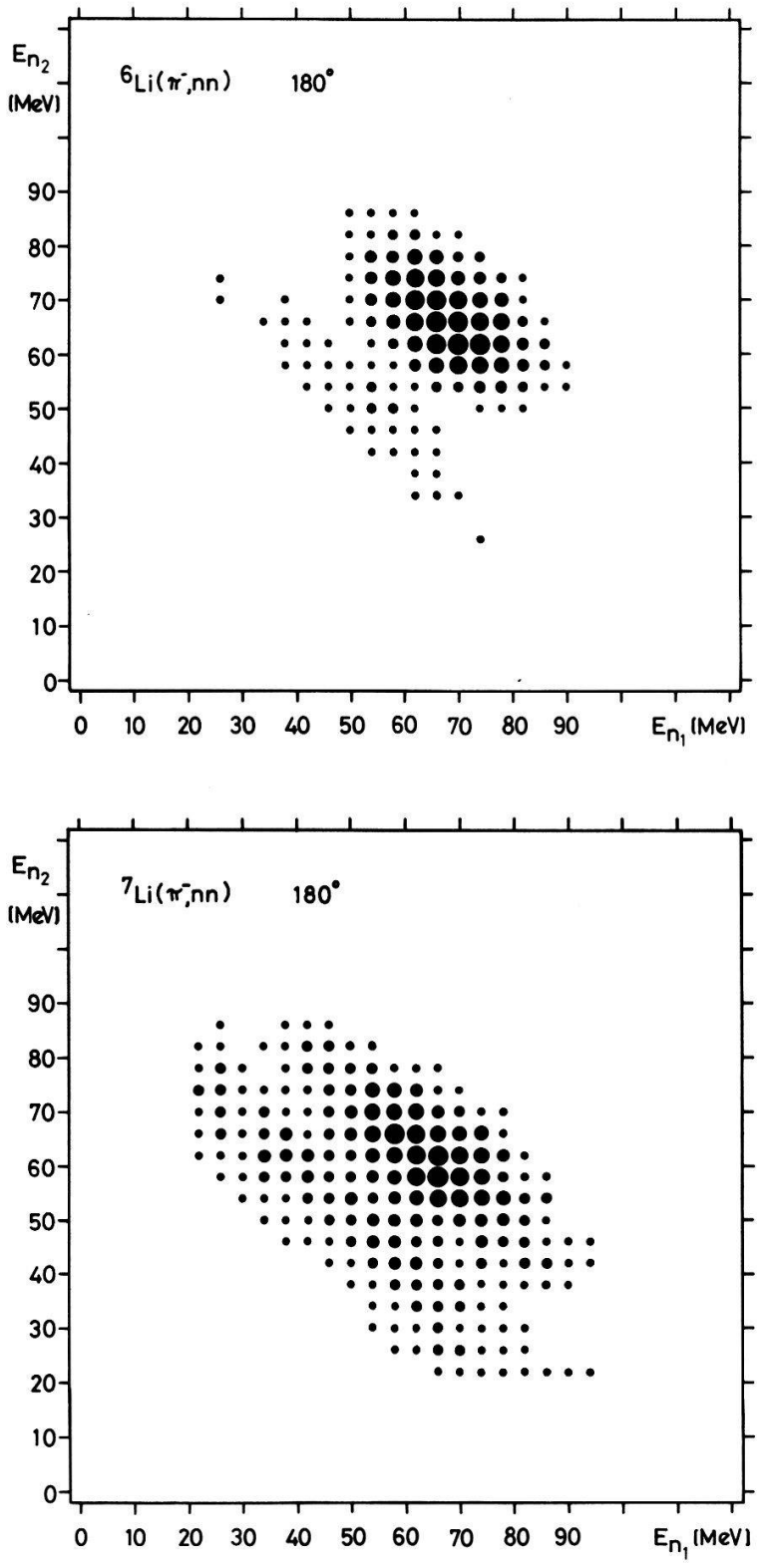

Figure 9
2-dim energy spectra of coincident neutrons (E_{n_1} and $E_{n_2} > 20$ MeV) emitted after the absorption of stopped negative pions in ^{6}Li and ^{7}Li for an opening angle of 180°. The area of the points is proportional to the intensity $d^3W/(dE_{n_1}\, dE_{n_2}\, d\cos\theta)$. Both spectra are normalized individually to the maximum of the 2-dim distribution. Points below 10% of the maximum are not plotted.

two dimensional energy spectra of coincident neutrons ($E_{n_1}, E_{n_2} > 20$ MeV) for an opening angle of 180°. The spectra of both isotopes are similar and show two characteristic regions of quasi-free absorption on an *np* pair in the nucleus, i.e. i] *p*-shell absorption: coincident $n-n$ events emitted after the primary absorption process, where both absorbing nucleons are from the *p*-shell, should result in a characteristic enhancement around $E_{n_1} = E_{n_2} = 67.5$ MeV and 64 MeV for ^{6}Li and ^{7}Li, respectively. This enhancement corresponds to a sum energy $E_s = E_n + E_{n_2} + E_r$ (E_r is the recoil energy of the residual nucleus) equal to the Q value of the corresponding reaction: $Q = 135$ MeV for $^6\text{Li}(\pi^-, nn)^4\text{He}$ and $Q = 128$ MeV for $^7\text{Li}(\pi^-, nn)^5\text{He}$. This enhancement is observed experimentally; it is broadened in the direction of constant $E_{n_1} + E_{n_e}$ due to the Fermi motion of the absorbing *np* pair. ii] *s*-shell absorption: coincident $n-n$ events emitted after the primary absorption process, where at least one or both absorbing nucleons are from the *s*-shell, should result in an enhancement at lower energies. In the experiment an enhancement is seen around $E_{n_1} = E_{n_2} = 54$ MeV and 52 MeV for ^{6}Li and ^{7}Li, respectively. The recoil corrected sum energy spectra for ^{6}Li and ^{7}Li are given in Fig. 10 for opening angles of 180°, 170° and 160°. Both enhancements mentioned above are clearly visible and show a strong angular dependence. The present sum energy spectra for ^{6}Li and ^{7}Li are in agreement with the sum energy or corresponding excitation energy spectra of Davies et al. [26] (for ^{6}Li and ^{7}Li), Calligaris et al. [27] (for ^{6}Li), and Bassalleck et al. [29] (for ^{6}Li and ^{7}Li). Because of the rather bad energy resolution, no *s*-shell enhancement was seen in Ref. [26]. Ref. [29] had a very good energy resolution and therefore had a better separation of *p*-shell and *s*-shell absorption. One can separate the *p*-shell from the *s*-shell processes by selecting specific regions in the sum energy spectra (see Fig. 10). In Fig. 11 the projections of the two dimensional energy spectra on one axis are

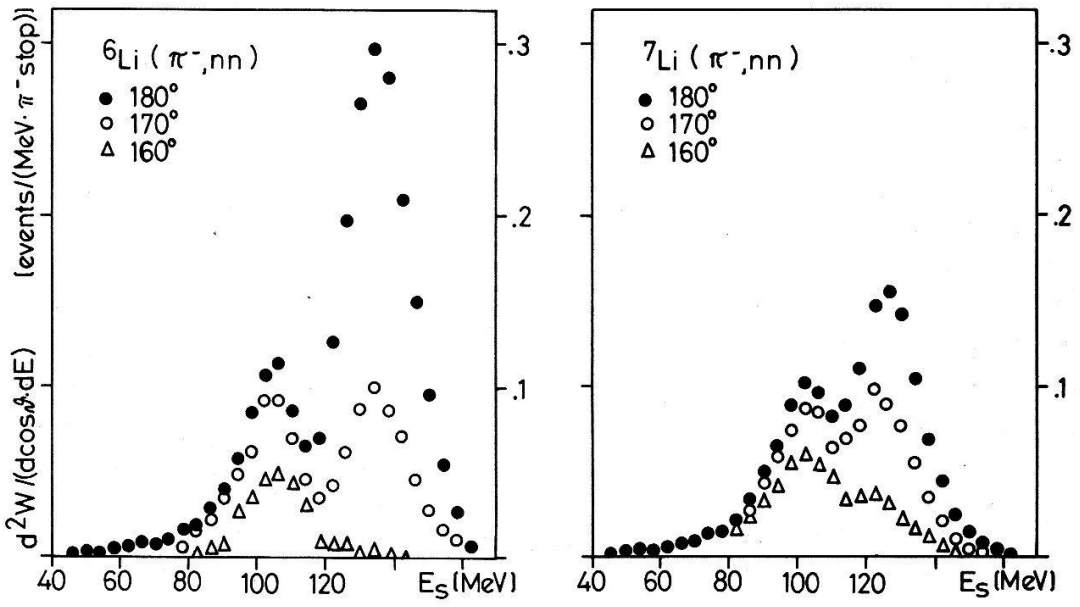

Figure 10
Recoil corrected sum energy spectra of two coincident neutrons ($E_{n_1}, E_{n_2} > 20$ MeV) emitted after the absorption of stopped negative pions in ^{6}Li and ^{7}Li for opening angles of 180°, 170° and 160°. Primary *p*-shell neutrons were defined by the condition $118 < E_s < 153$ MeV for ^{6}Li and $114 < E_s < 146$ MeV for ^{7}Li. Primary *s*-shell neutrons were defined by $82 < E_s < 118$ MeV for ^{6}Li and $82 < E_s < 114$ MeV for ^{7}Li.

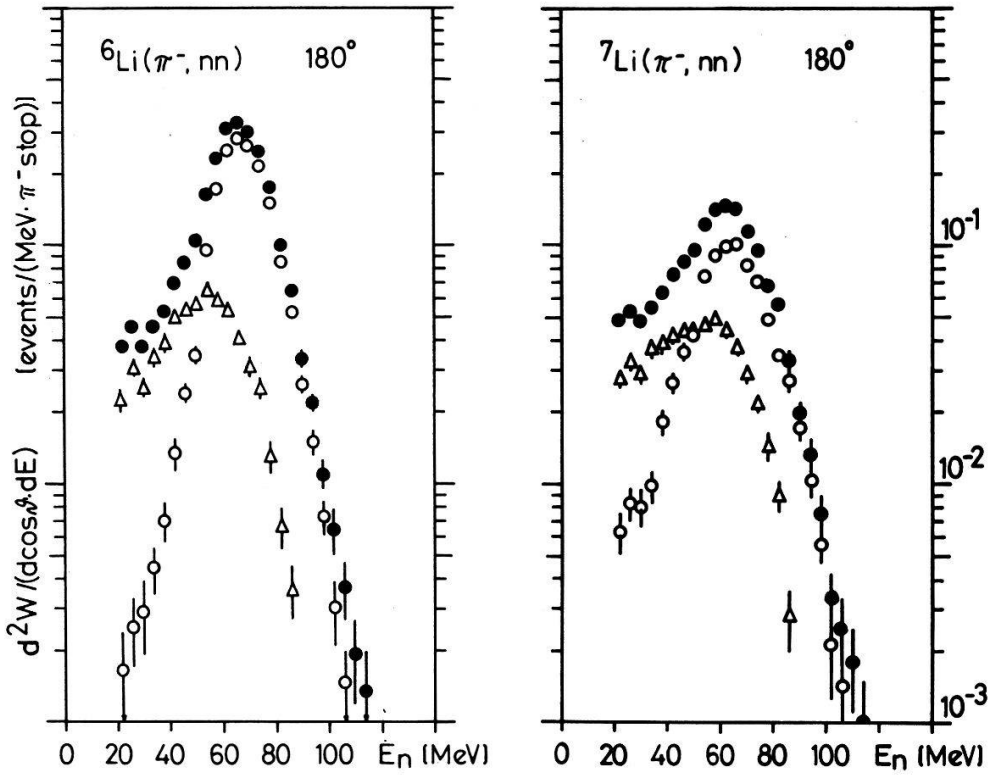

Figure 11
1-dim neutron energy spectra of coincident neutrons (E_{n_1}, $E_{n_2} > 20$ MeV) emitted after the absorption of stopped negative pions in ^{6}Li and ^{7}Li for an opening angle of 180°. The spectra were obtained from the 2-dim spectra (Fig. 9) by taking the mean of the projections on the E_{n_1}, E_{n_2} axis. The full circles represent the spectrum of all neutrons; the open circles depict the spectrum of neutrons from p-shell absorption; open triangles that of neutrons from s-shell absorption. p-shell and s-shell neutrons were defined by the recoil corrected sum energy E_s (see Fig. 10). The errors shown are statistical only, the error in normalization is 15%.

given for ^{6}Li and ^{7}Li, respectively, for an opening angle of 180°. The figures show the one dimensional energy spectra of all coincident neutrons (E_{n_1}, $E_{n_2} > 20$ MeV), neutrons from s-shell absorption and neutrons from p-shell absorption. The primary p-shell spectra are symmetric with respect to the energy $Q/2 = 67.5$ MeV and 64 MeV for ^{6}Li and ^{7}Li, respectively, and are of similar shape; the full widths are 22.2 MeV FWHM for ^{6}Li and 26.3 MeV FWHM for ^{7}Li (in Ref. [29] widths of 18.5 MeV and 30 MeV FWHM are obtained for ^{6}Li and ^{7}Li, respectively). The opening angle distributions for $n-n$ events emitted after p-shell and s-shell absorption in ^{6}Li and ^{7}Li are shown in Fig. 12. All opening angle distributions are peaked at 180°, the p-shell being more sharply peaked than the corresponding s-shell distributions. The half widths are 7.2° and 10.5° HWHM for the p-shell and 17.6° and 23.5° HWHM for the s-shell $n-n$ opening angle distributions of ^{6}Li and ^{7}Li, respectively. The widths of the total opening angle distributions (E_{n_1}, $E_{n_2} > 20$ MeV), with no restriction on the sum energy, are 8.3° and 14.6° HWHM for ^{6}Li and ^{7}Li, respectively. The experimental opening angle distributions are compared with the results of Ref. [29] (Fig. 12). Ref. [29] had better energy and angular resolution, on the other hand the range of opening angles is much larger in the present work. Because the data of Ref. [29] is not absolutely normalized, the distributions were normalized individually to the

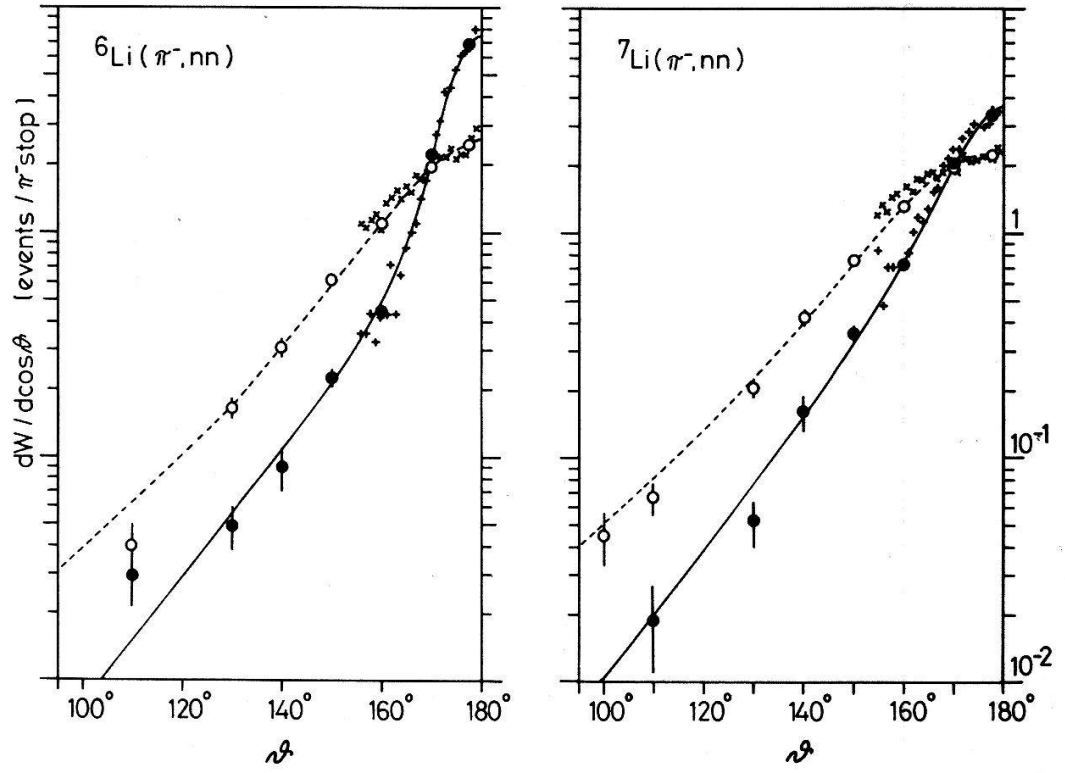

Figure 12
Opening angle distributions for p-shell (full circles) and s-shell (open circles) $n-n$ events (E_{n_1}, $E_{n_2}>20$ MeV) emitted after the absorption of stopped negative pions in ^{6}Li and ^{7}Li. p-shell and s-shell neutrons were defined by the recoil corrected sum energy E_s (see Fig. 10). The solid and dashed lines represent the fits, which were made to the data. The data of Ref. [29] (plus signs and crosses) which is not absolutely normalized, was normalized to the 180° point and is shown for comparison. The errors shown are statistical only, the error in normalization is 15%.

present 180° point. The agreement with the data of Ref. [29] is good for both the p-shell and s-shell opening angle distributions. In Fig. 13 the present total opening angle distributions for all neutrons with E_{n_1}, $E_{n_2}>15$ MeV are compared with the measurements of Davies et al. [26] (for ^{6}Li and ^{7}Li), Nordberg et al. [11] (for ^{6}Li) and Bassalleck et al. [29] (for ^{6}Li and ^{7}Li). The agreement with Refs. [11, 26, 29] is good, taking into account the large uncertainties of the older measurements [11, 26]. The experimental widths of the opening angle distributions are 8.6° and 15.8° HWHM for ^{6}Li and ^{7}Li, respectively.

In order to allow the integration of the opening angle distributions the data were fitted to the following formula:

$$\frac{dW}{d\cos\theta} = a_1 \cdot \exp\left(-\frac{1}{2}\left(\frac{\theta-180°}{a_2}\right)^2\right) + a_3 \cdot \exp(a_4\theta).$$

The fits to the data are indicated in Figs. 12, 13. The integrated yields of coincident $n-n$ events emitted after pion absorption in ^{6}Li and ^{7}Li are given in Table 2 for different energy thresholds, as well as for p-shell and s-shell components. The values quoted were obtained from the fits to the data integrated over all opening angles from 0° to 180°. For ^{6}Li and ^{7}Li 0.16 ± 0.03 and 0.18 ± 0.03 p-shell and 0.28 ± 0.05 and 0.34 ± 0.05 s-shell $n-n$ events are emitted per stopped pion, respectively. The multiplicities of coincident neutrons with energies higher than 20 MeV are 0.51 ± 0.09 and 0.61 ± 0.10 $n-n$ events per

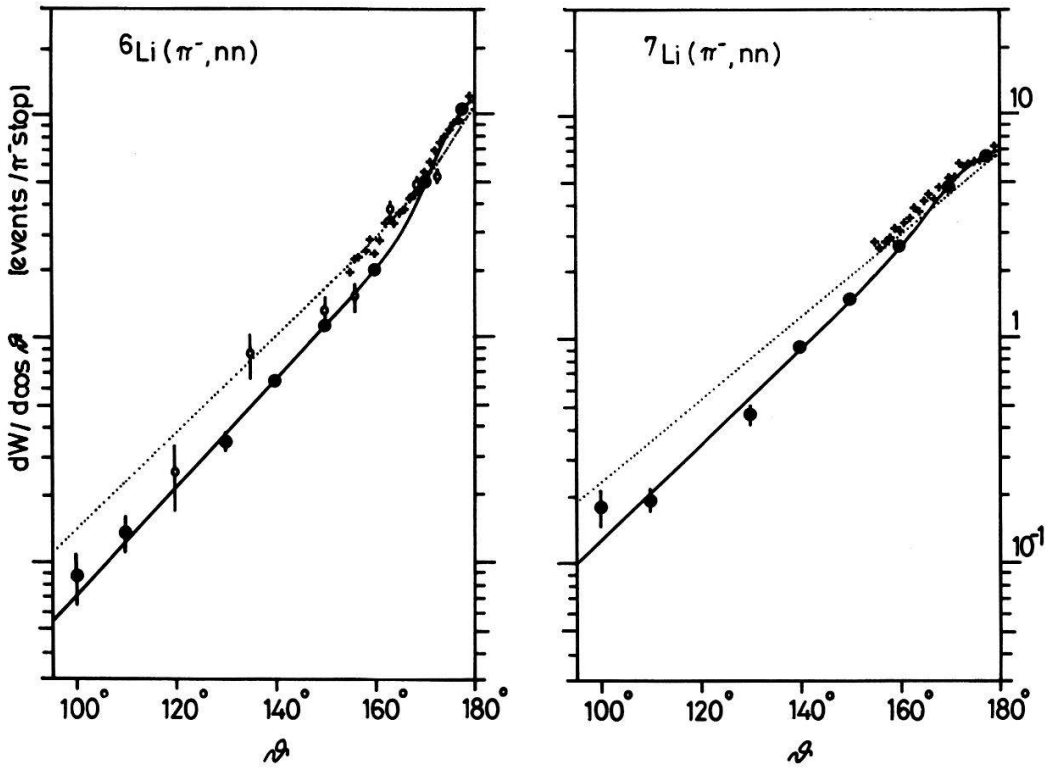

Figure 13
Opening angle distributions (large full circles) for $n-n$ events ($E_{n_1}, E_{n_2} > 15$ MeV) emitted after the absorption of stopped negative pions in ^{6}Li and ^{7}Li are compared with the measurements of Ref. [26] (dotted lines), Ref. [11] (small open circles for ^{6}Li) and Ref. [29] (plus signs). The solid lines represent the fits, which were made to the data. The data of Refs. [26, 29] were normalized to the 180° point; the data of Ref. [11] to the 170° point.

stopped pion for ^{6}Li and ^{7}Li, respectively. Comparing the above numbers with the sum of both p-shell and s-shell $n-n$ events (0.44 ± 0.06 for ^{6}Li and 0.52 ± 0.06 for ^{7}Li) shows that for ^{6}Li and ^{7}Li most high energy $n-n$ coincidences stem from the primary absorption process and not from secondary processes. In fact in ^{6}Li and ^{7}Li almost all absorption processes lead to the emission of highly energetic ($E > 20$ MeV) particle pairs [6]. For comparison, data from Davies et al. [26], Nordberg et al. [11], Calligaris et al. [27] and Bassalleck et al. [29] are also tabulated. The agreement is generally good. Only the measurements of Ref. [26] are somewhat higher, probably because of the bad energy resolution and the slightly different cuts in the sum energy. Therefore, the quoted numbers of Ref. [26] for p-shell n-n events should more likely be compared with the present sum of p-shell and s-shell $n-n$ events. The data of Ref. [29] cover only opening angles between 155° and 180° and are, therefore, lower limits for the total multiplicities. Integrating the present opening angle distributions between 155° and 180° yields the following results: 0.12 ± 0.02 p-shell $n-n$ events for both ^{6}Li and ^{7}Li; 0.13 ± 0.02 and 0.14 ± 0.02 s-shell $n-n$ events for ^{6}Li and ^{7}Li, respectively, in good agreement with the data of Ref. [29].

3.2.2. *Results for* ^{12}C, ^{59}Co *and* ^{197}Au. Two dimensional neutron-neutron energy spectra and neutron-neutron opening angle distributions were measured for pion absorption in ^{12}C, ^{59}Co and ^{197}Au for opening angles θ from 50° to 180°.

Table 2
Measured multiplicities X_m of coincident $n-n$ events emitted per stopped pion after the absorption of stopped negative pions in ^{6}Li and ^{7}Li are compared with other results. Multiplicities are tabulated for different energy thresholds, as well as for p-shell and s-shell absorption. Primary p-shell and s-shell $n-n$ events were defined by the recoil corrected sum energy E_s (see Fig. 10). The errors quoted for this work contain statistical errors of the fit to the opening angle distributions and an error in absolute normalization of 15%.

Target	X_m $E_{n_1}>10$ MeV $E_{n_2}>10$ MeV	X_m $E_{n_1}>15$ MeV $E_{n_2}>15$ MeV	X_m $E_{n_1}>20$ MeV $E_{n_2}>20$ MeV	X_m $E_{n_1}>30$ MeV $E_{n_2}>30$ MeV	X_m $E_{n_1}>40$ MeV $E_{n_2}>40$ MeV	X_m primary p-shell	x_m Primary s-shell	Reference
^{6}Li	0.73(14)	0.60(10)	0.51(9)	0.36(7)	0.24(5)	0.16(3)	0.28(5)	This work
						>0.10	>0.15	Ref. [29][a])
			0.55(8)					Ref. [27][b])
			0.41(17)					Ref. [11]
			0.69(28)					Ref. [11]
						0.37(10)		Ref. [26][c])
^{7}Li	1.03(19)	0.78(13)	0.61(10)	0.39(7)	0.24(5)	0.18(3)	0.34(5)	This work
						>0.10	>0.13	Ref. [29][a])
			0.50(21)					Ref. [11]
						0.50(12)		Ref. [26][c])

[a]) Ref. [29] does not give any absolute $n-n$ multiplicities for ^{6}Li and ^{7}Li. The multiplicities quoted in the table were determined from the absolutely normalized excitation energy spectra of Ref. [29], using the same cuts in E_s as in this work. Since the angular range in Ref. [29] covered only opening angles between 155° and 180°, the numbers given in the table are lower limits only.

[b]) The data of Ref. [27] is not absolutely normalized, only the relative value of ^{6}Li to ^{12}C is given (the value quoted in the table for ^{6}Li was normalized to ^{12}C, which was set to the present value of 0.27 ± 0.04 for $E_{n_1}, E_{n_2}>20$ MeV).

[c]) In Ref. [26] slightly different definitions for p-shell events were used.

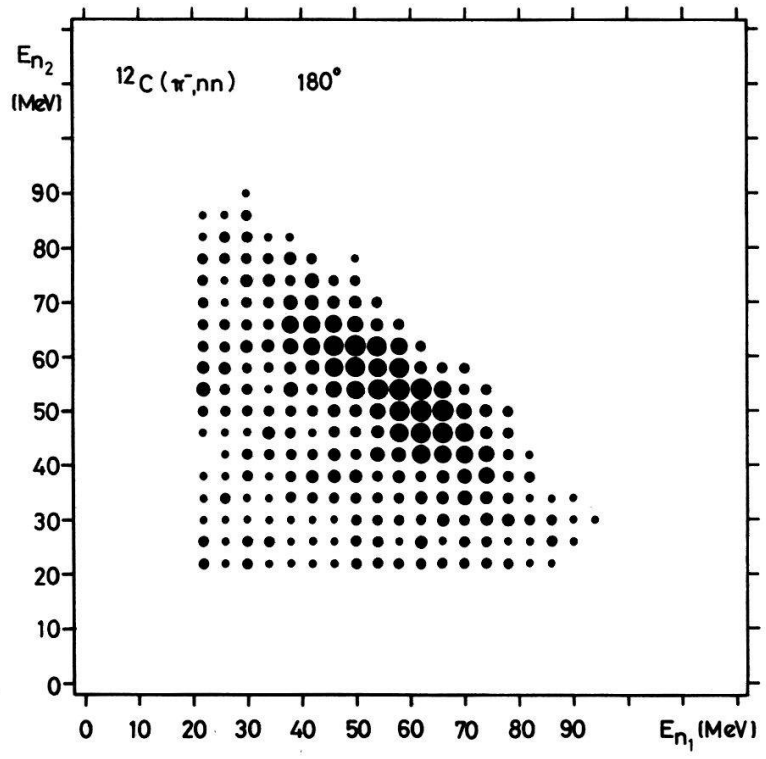

Figure 14
2-dim energy spectra of coincident neutrons (E_{n_1} and $E_{n_2} > 20$ MeV) emitted after the absorption of stopped negative pions in ^{12}C for an opening angle of 180°. The area of the points is proportional to the intensity. The spectrum is normalized to the maximum of the 2-dim distribution. Points below 10% of the maximum are not plotted.

Although these targets have been measured earlier by Hartmann et al. [21], the present measurements cover a wider range of opening angles and, for ^{12}C, have better statistics than the previous measurements [11, 21, 28, 30]. Fig. 14 shows the two dimensional energy spectra of coincident neutrons (E_{n_1}, $E_{n_2} > 20$ MeV) emitted after the absoption of stopped negative pions in ^{12}C for an opening angle of 180°. The spectrum shows the characteristic region of primary p-shell absorption on an np pair around $E_{n_1} = E_{n_2} = 56$ MeV, corresponding to a sum energy E_s equal to the Q value of the reaction: $Q = 112$ MeV for $^{12}C(\pi^-, nn)^{10}B$. As compared with ^6Li and ^7Li, primary s-shell absorption is greatly reduced in ^{12}C and secondary processes are more important. The recoil corrected sum energy spectrum for ^{12}C is given in Fig. 15 for opening angles of 180°, 160° and 140°. The present sum energy spectrum for ^{12}C is in agreement with the corresponding excitation energy spectra of Calligaris et al. [27], Cheshire et al. [28] and Bassalleck et al. [30]. Fig. 16 shows the one dimensional energy spectra of all coincident neutrons (E_{n_1}, $E_{n_2} > 20$ MeV), and primary p-shell $n-n$ events. As for ^6Li and ^7Li, the p-shell neutron spectrum of ^{12}C is symmetric with respect to the energy $Q/2 = 56$ MeV and has a width of 37.6 MeV FWHM. The opening angle distributions for $n-n$ events (E_{n_1} and $E_{n_2} > 20$ MeV), emitted after pion absorption in ^{12}C, ^{59}Co and ^{197}Au are shown in Fig. 17. The opening angle distributions are peaked at 180°, the widths of the distributions increase with increasing mass number A: the widths are 25°, 40° and 53° HWHM for ^{12}C, ^{59}Co and ^{197}Au, respectively. For ^{12}C the width of the p-shell component alone is 20° HWHM.

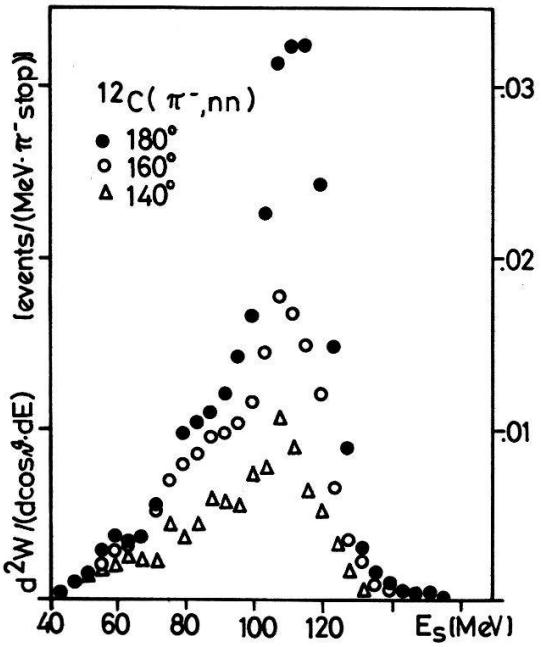

Figure 15
Recoil corrected sum energy spectra of two coincident neutrons (E_{n_1}, $E_{n_2} > 20$ MeV) emitted after the absorption of stopped negative pions in ^{12}C for opening angles of 180°, 160° and 140°. Primary p-shell neutrons were defined by the condition $90 < E_s < 128$ MeV.

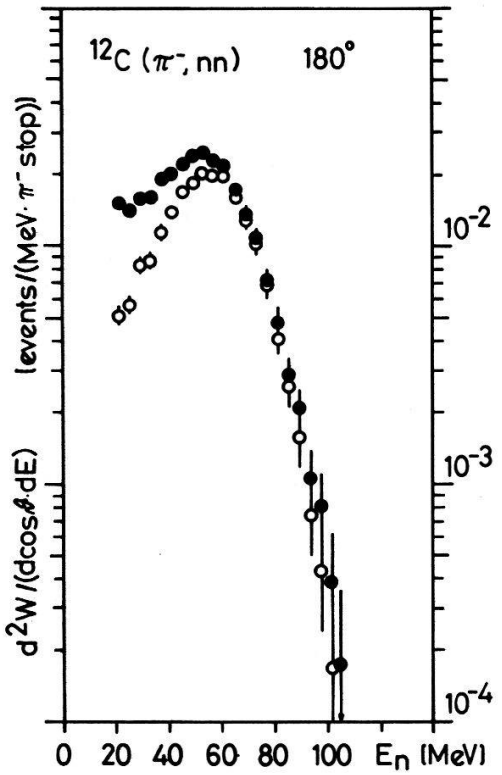

Figure 16
1-dim neutron energy spectra of coincident neutrons (E_{n_1}, $E_{n_2} > 20$ MeV) emitted after the absorption of stopped negative pions in ^{12}C for an opening angle of 180°. The spectra were obtained from the 2-dim spectrum (Fig. 14) by taking the mean of the projections on the E_{n_1}, E_{n_2} axis. The full circles represent the spectrum of all neutrons; the open circles depict the spectrum of p-shell neutrons, defined by the recoil corrected sum energy E_s (see Fig. 15).

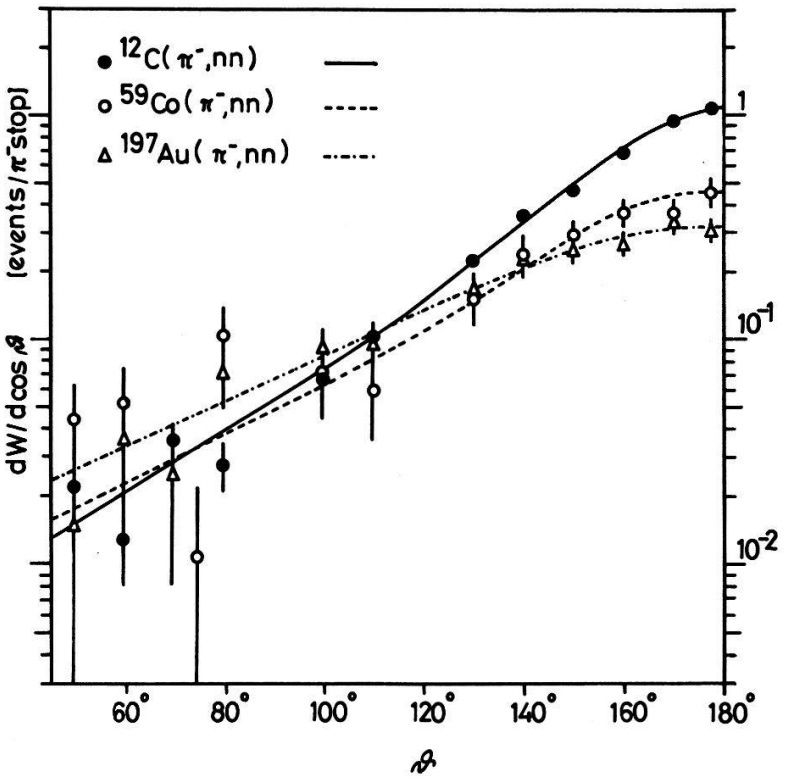

Figure 17
Opening angle distributions for $n-n$ coincidence events ($E_{n_1}, E_{n_2} > 20$ MeV) emitted after the absorption of stopped negative pions in ^{12}C, ^{59}Co and ^{197}Au. The solid (^{12}C), dashed (^{59}Co) and dot-dashed (^{197}Au) lines represent the fits, which were made to the data.

The present opening angle distributions agree in spectral shape very well with the data of Ref. [21], where the widths are 30°, 45° and 50° HWHM for ^{12}C, ^{59}Co and ^{197}Au, respectively. Also the absolute yields (Table 3) for all three targets are in good agreement. In Fig. 18, the opening angle distributions ($E_{n_1}, E_{n_2} > 15$ MeV) are compared with the results of Bassalleck et al. [30] (for ^{12}C and ^{16}O), Hartmann et al. [21] (for ^{12}C) and Nordberg et al. [11] (for ^{16}O). The data of Refs. [11, 30] were normalized to the present 180° and 170° point, respectively. There is a serious disagreement with the ^{12}C data of Ref. [30], which shows hardly any angular dependence. The agreement with the ^{16}O data of Ref. [30], however, is good for opening angles larger than about 140°. There is agreement with the ^{16}O data of Ref. [11] within the quite large errors. The integrated yields of coincident $n-n$ events emitted after pion absorption in ^{12}C, ^{59}Co and ^{197}Au are given in Table 3 for different energy thresholds, and in the case of ^{12}C for primary p-shell $n-n$ events. The values quoted were obtained from the fits to the data integrated over all opening angles from 0° to 180°. The fits to the data are indicated in Figs. 17, 18. For ^{12}C 0.16 ± 0.03 primary p-shell $n-n$ events are emitted per stopped pion. The multiplicities of coincident neutrons with energies higher than 20 MeV are 0.27 ± 0.04, 0.19 ± 0.04 and 0.19 ± 0.04 $n-n$ events per stopped pion for ^{12}C, ^{59}Co and ^{197}Au, respectively. Comparing the above number for ^{12}C with that of primary $n-n$ events indicates that for ^{12}C secondary processes are of about equal importance as primary processes. In fact the probability for the emission of highly energetic particle pairs ($E > 20$ MeV) is only about 50% per stopped pion [6].

Table 3
Measured multiplicities X_m of coincident $n-n$ events emitted per stopped pion after the absorption of stopped negative pions in ^{12}C, ^{59}Co and ^{197}Au are compared with other results. Multiplicities are tabulated for different energy thresholds, as well as for p-shell absorption. For ^{12}C primary p-shell $n-n$ events were defined by the recoil corrected sum energy E_s (see Fig. 15)

Target	X_m $E_{n_1}>10$ MeV $E_{n_2}>10$ MeV	X_m $E_{n_1}>15$ MeV $E_{n_2}>15$ MeV	X_m $E_{n_1}>20$ MeV $E_{n_2}>20$ MeV	X_m $E_{n_1}>30$ MeV $E_{n_2}>30$ MeV	X_m $E_{n_1}>40$ MeV $E_{n_2}>40$ MeV	X_m primary p-shell	Reference
^{12}C	0.46(8)	0.36(6)	0.27(4)	0.15(3)	0.08(2)	0.16(3)	This work
	0.46(7)	0.36(6)	0.26(4)	0.15(2)	0.08(1)		Ref. [21][a]
		>0.26				>0.13	Ref. [30][b]
			0.14(6)				Ref. [11]
						$>0.022(^{+8}_{-3})$	Ref. [28][c]
^{14}N						$>0.07(^{+4}_{-2})$	Ref. [30][b]
			0.14(6)				Ref. [11]
^{16}O		>0.10				>0.05	Ref. [30][b]
			0.27(11)				Ref. [11]
			0.39(16)				Ref. [11]
^{59}Co	0.47(9)	0.29(5)	0.19(4)	0.11(2)	0.05(1)		This work
	0.31(7)	0.26(6)	0.20(5)	0.11(3)	0.04(1)		Ref. [21][a]
^{nat}Cu			0.08(5)				Ref. [11]
^{197}Au	0.39(7)	0.27(5)	0.19(4)	0.11(2)	0.05(1)		This work
	0.32(7)	0.28(6)	0.22(5)	0.12(2)	0.04(1)		Ref. [21][a]
^{nat}Pb			0.06(6)				Ref. [11]

a) The integration of the $n-n$ opening angle distribution of Ref. [21] is wrong by a factor of 2. The numbers quoted for ^{12}C, ^{59}Co and ^{197}Au (Ref. [21]) were therefore multiplied by 2; for ^{12}C a further correction was necessary due to the fact that in Ref. [21] too much isotropic background was subtracted, because no measurements below 90° were available (the multiplicities for $n-n$ events with opening angles smaller than 90° were taken from this work).

b) In Ref. [30] no primary $n-n$ multiplicities are given for ^{12}C and ^{16}O; the numbers quoted were determined from the absolutely normalized excitation energy spectra, using the same cuts in E_s as in this work. Since the angular range in Ref. [30] covered only opening angles between 145° and 180° (for ^{12}C and ^{14}N) and 155° to 180° (for ^{16}O), the multiplicities given in the table are lower limits only.

c) The value quoted in the table is taken from Ref. [28] as quoted in Ref. [12] and is a lower limit because it covers only angles between 170° and 180°.

Thus final-state interactions of the absorbing nucleons with the residual nucleus seem to be important in a nucleus as light as ^{12}C. For comparison, the data of Nordberg et al. [11], Bassalleck et al. [30] and Hartmann et al. [21] are also tabulated. The agreement with the data of Ref. [21] is good. For ^{12}C there is agreement with the data of Ref. [11] within the large errors quoted. In Ref. [11] the mean of all measured targets from ^{9}Be to ^{16}O is 0.23 ± 0.04 $n-n$ events per stopped pion. The ^{nat}Cu and ^{nat}Pb measurements of Ref. [11] have very large errors and therefore, give only qualitative results. The data quoted from Ref. [30] for p-shell neutrons were determined from the absolutely normalized excitation energy spectra, and correspond to the sum energy cuts used in this work. The data, however, cover only opening angles between 145° and 180° (for ^{12}C and ^{14}N) or 155° to 180° (for ^{16}O) and are therefore only lower limits for the total multiplicities. The numbers may be compared with the present results for

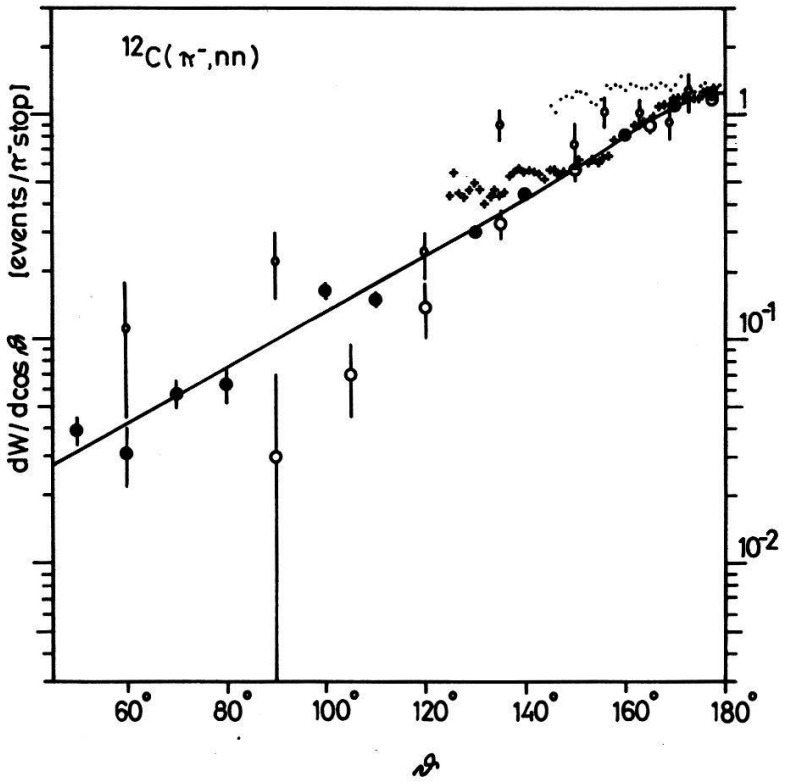

Figure 18
Present opening angle distributions (large full circles) for $n-n$ events ($E_{n_1}, E_{n_2} > 15$ MeV) emitted after the absorption of stopped negative pions in ^{12}C are compared with the measurements of Ref. [21] (large open circles for ^{12}C), Ref. [11] (small circles for ^{16}O) and Ref. [30] (plus signs for ^{16}O and small points for ^{12}C). The solid line represents the fit, which was made to the data. The data of Ref. [30] were normalized to the 180° point; the data of Ref. [11] to the 170° point. The data of Ref. [21] are absolutely normalized; the isotropic background is subtracted (see also Table 3).

^{12}C, using the corresponding angular range: 0.08 ± 0.02 and 0.05 ± 0.01 $n-n$ events per stopped pion for an angular range from 145° or 155° to 180°, respectively. There is good agreement with the ^{14}N and ^{16}O data and disagreement with the ^{12}C data of Ref. [30]. $n-n$ multiplicities for ^{12}C with $E_{n_1}, E_{n_2} >$ 15 MeV from this work are: 0.36 ± 0.06, 0.13 ± 0.02 and 0.09 ± 0.02 $n-n$ events per stopped pion for an angular range from 0°, 145° or 155° to 180°, respectively. Again there is good agreement with the ^{16}O data and disagreement with the ^{12}C data of Ref. [30]. The data of Cheshire and Sobottka [28] for ^{12}C (as quoted in Ref. [12]) cover an angular range from 170° to 180° and are therefore lower limits only. The present data integrated between 170° and 180° gives 0.011 ± 0.002 $n-n$ events per stopped pion, in disagreement with the number quoted from Ref. [28]. The data of Ref. [28] was used by Lee et al. [12] to determine the ratio R of absorbing np to pp pairs from the p-shell, $R = 16^{+8}_{-3}$. Taking the present nn yield and the np yield of Lee et al. [12] one obtains a ratio $R = 8^{+4}_{-2}$. This number is in agreement with the ratio determined in Ref. [6], namely $R = 5.6 \pm 1.2$.

3.3. *Concluding remarks*

The one and two dimensional neutron energy spectra and neutron-neutron opening angle distributions measured in this work are in general agreement with

existing measurements and offer a reliable set of data for ^{6}Li, ^{7}Li, ^{12}C, ^{59}Co and ^{197}Au. The present results are in agreement with the two nucleon absorption mechanism; in the coincident measurements absorption on *p*- and *s*-shell nucleons has been detected. Together with the charged particle energy spectra [5, 14], charged particle-charged particle coincidence measurements [14] and the neutron-charged particle coincidence measurements, which will soon become available (first results are given in Ref. [6]), a complete set af data will exist for the above mentioned nuclei, thus allowing specific conclusions on pion absorption to be made, namely on experimental ratios R and the importance of cluster absorption.

We would like to thank W. Bertl, H. Brechbühl and C. Grab for their participation during the preparation of the experiment and the data taking, A. Zglinski for his help in writing the off-line analysis programm and P. Vernin for supplying us with the neutron detection efficiency code.

REFERENCES

[1] N. C. Mukhopadhyay, J. Hadermann and K. Junker, Nucl. Phys. *A319* (1979) 448.
[2] F. Hachenberg, H. C. Chiang and J. Hüfner, Phys. Lett. *97B* (1980) 18; H. C. Chiang and J. Hüfner, Nucl. Phys. *A352* (1981) 442; F. Hachenberg, Phys. Lett. *113B* (1982) 451.
[3] E. Gadioli and E. Gadioli-Erba, Nucl. Phys. *A256* (1976) 414; Phys. Rev. *C16* (1977) 1404.
[4] A. S. Iljinov and V. I. Nazaruk, Nucl. Phys. *A268* (1976) 513; V. S. Buttsev, A. S. Iljinov and S. E. Chigrinov, Sov. J. Part. and Nucl. *11* (1980) 358.
[5] H. S. Pruys, R. Engfer, H. P. Isaak, T. Kozlowski, U. Sennhauser, H. K. Walter and A. Zglinski, Proc. Intermediate Energy Nuclear Chemistry Workshop, Los Alamos Report LA-8835-C (1981) 240.
[6] P. Heusi, H. P. Isaak, H. S. Pruys, R. Engfer, U. Sennhauser and H. K. Walter, SIN preprint PR 82–11 (1982) and Contribution to the 3rd International Conference on Nuclear Reaction Mechanisms, Varenna (1982), P. Heusi, thesis Univ. Zürich 1982.
[7] K. J. LeCouteur, Proc. Phys. Soc. *A65* (1952) 718.
[8] H. S. Pruys, R. Engfer, R. Hartmann, U. Sennhauser, H. J. Pfeiffer, H. K. Walter, J. Morgenstern, A. Wyttenbach, E. Gadioli and E. Gadioli-Erba, Nucl. Phys. *A316* (1979) 365; C. J. Orth, W. R. Daniels, B. J. Dropesky, R. A. Williams, G. C. Giesler and J. N. Ginocchio, Phys. Rev. *C21* (1980) 2524.
[9] H. P. Isaak, A. Zglinski, R. Engfer, R. Hartmann, E. A. Hermes, H. S. Pruys, F. W. Schlepütz, T. Kozlowski, U. Sennhauser, H. K. Walter, K. Junker and N. C. Mukhopadhyay, Nucl. Phys. *A392* (1983) 368; H. P. Isaak, H. S. Pruys, R. Engfer, R. Hartmann, E. A. Hermes, F. W. Schlepütz, A. Zglinski, T. Kozlowski, U. Sennhauser and H. K. Walter, Nucl. Phys. *A392* (1983) 385.
[10] D. Gotta, M. Dörr, W. Fetscher, G. Schmidt, H. Ullrich, G. Backenstoss, W. Kowald, I. Schwanner and H. J. Weyer, Phys. Lett. *112B* (1982) 129; S. Ozaki, R. Weinstein, G. Glass, E. Loh, L. Neimala, A. Wattenberg, Phys. Rev. Lett. *4* (1960) 533.
[11] M. E. Nordberg, Jr., K. F. Kinsey and R. L. Burman, Phys. Rev. *165* (1968) 1096.
[12] D. M. Lee, R. C. Minehart, S. E. Sobottka and K. O. H. Ziock, Nucl. Phys. *A182* (1972) 20; Nucl. Phys. *A197* (1972) 106.
[13] K. Shimizu and A. Faessler, Nucl. Phys. *A333* (1980) 495.
[14] H. S. Pruys, R. Engfer, R. Hartmann, E. A. Hermes, H. P. Isaak, F. W. Schlepütz, U. Sennhauser, W. Dey, K. Hess, H. J. Pfeiffer, H. K. Walter and W. Hesselink, Nucl. Phys. *A352* (1981) 388; U. Sennhauser, H. J. Pfeiffer, H. K. Walter, F. W. Schlepütz, H. S. Pruys, R. Engfer, R. Hartmann, E. A. Hermes, P. Heusi, H. P. Isaak, and W. H. A. Hesselink, Nucl. Phys. *A386* (1982) 429; U. Sennhauser, W. Dey, H. J. Pfeiffer, H. K. Walter, H. S. Pruys, F. W. Schlepütz, R. Engfer, R. Hartmann, E. A. Hermes, P. Heusi, H. P. Isaak, and W. H. A. Hesselink, Nucl. Phys. *A386* (1982) 447.
[15] G. F. Bertsch and D. O. Riska, Phys. Rev. *C18* (1978) 317.
[16] K. O. H. Ziock, C. Cernigoi, G. Gorini, Phys. Lett. *33B* (1970) 471; P. J. Castleberry, L. Coulson, R. C. Minehart and K. O. H. Ziock, Phys. Lett. *34B* (1971) 57; Yu G. Budyashov, V. G. Zinov, A. D. Konin, N. V. Rabin, A. M. Chatrchyan, Sov. Phys. JETP *35* (1972) 13.

[17] V. M. KOLYBASOV, Sov. Jour. Nucl. Phys. *3* (1966) 535, 704; V. M. KOLYBASOV and V. A. TSEPOV, Sov. Jour. Nucl. Phys. *14* (1972) 418.
[18] G. C. VENUTI, G. FRONTEROTTA and G. MATTHIAE, Phys. Lett. *9* (1964) 45, Nuovo Cimento *34* (1964) 1446.
[19] H. L. ANDERSON, E. P. HINCKS, C. S. JOHNSON, C. REY and A. M. SEGAR, Phys. Rev. *133* (1964) B392.
[20] P. M. HATTERSLEY, H. MUIRHEAD and J. N. WOULDS, Nucl. Phys. *67* (1965) 309.
[21] R. HARTMANN, H. P. ISAAK, R. ENGFER, E. A. HERMES, H. S. PRUYS, W. DEY, H. J. PFEIFFER, U. SENNHAUSER, H. K. WALTER and J. MORGENSTERN, Nucl. Phys. *A308* (1978) 345.
[22] U. KLEIN, G. BÜCHE, W. KLUGE, H. MATTHÄY and G. MECHTERSHEIMER, Nucl. Phys. *A329* (1979) 339.
[23] R. MADEY, T. VILAITHONG, B. D. ANDERSON, J. N. KNUDSON, T. R. WITTEN, A. R. BALDWIN, and F. M. WATERMAN, Phys. Rev. *C25* (1982) 3050.
[24] B. BASSALECK, H. D. ENGELHARDT, E. L. HAASE, W. D. KLOTZ, C. W. LEWIS, F. TAKEUTCHI, H. ULLRICH, M. FURIC, Nucl. Phys. *A319* (1979) 397.
[25] C. CERNIGOI, I. GABRIELLI, N. GRION, G. PAULI, B. SAITTA, R. A. RICCI, P. BOCCACCIO and G. VIESTI, Nucl. Phys. *A352* (1981) 343.
[26] H. DAVIES, H. MUIRHEAD and J. N. WOULDS, Nucl. Phys. *78* (1966) 663.
[27] F. CALLIGARIS, C. CERNIGOI, I. GABRIELLI and F. PELLEGRINI, Nucl. Phys. *A126* (1969) 209.
[28] D. L. CHESHIRE and S. E. SOBOTTKA, Phys. Lett. *30B* (1969) 244; Nucl. Phys. *A146* (1970) 129.
[29] B. BASSALLECK, E. L. HAASE, W. D. KLOTZ, F. TAKEUTCHI, H. ULLRICH, M. FURIC and Y. SAKAMOTO, Phys. Rev. *C19* (1979) 1893.
[30] B. BASSALLECK, H. D. ENGELHARDT, E. L. HAASE, W. D. KLOTZ, C. W. LEWIS, F. TAKEUTCHI, H. ULLRICH and M. FURIC, Phys. Lett. *65B* (1976) 128; B. BASSALLECK, Ph.D. thesis (1977) University of Karlsruhe, unpublished. B. BASSALLECK, W. D. KLOTZ, F. TAKEUTCHI, H. ULLRICH and M. FURIC, Phys. Rev. *C16* (1977) 1526; B. BASSALLECK, H. D. ENGELHARDT, W. D. KLOTZ, C. W. LEWIS, F. TAKEUTCHI, H. ULLRICH and M. FURIC, Nucl. Phys. *A343* (1980) 365.
[31] B. BASSALLECK, W. D. KLOTZ, F. TAKEUTCHI, H. ULLRICH and M. FURIC, Zeitschrift für Physik *A286* (1978) 401.
[32] R. J. BARRETT, J. MCCARTHY, R. C. MINEHART and K. ZIOCK, Nucl. Phys. *A216* (1973) 145.
[33] J. COMISO, T. MEYER, F. SCHLEPÜTZ, K. O. H. ZIOCK, Phys. Rev. Lett. *35* (1975) 13; F. W. SCHLEPÜTZ, J. C. COMISO, T. C. MEYER and K. O. H. ZIOCK, Phys. Rev. *C19* (1979) 135; G. MECHTERSHEIMER, G. BÜCHE, U. KLEIN, W. KLUGE, H. MATTHÄY, D. MÜNCHMEYER and A. MOLINE, Nucl. Phys. *A324* (1979) 379; H. RANDOLL, H. I. AMOLS, W. KLUGE, H. MATTHÄY, A. MOLINE and D. MÜNCHMEYER, Nucl. Phys. *A381* (1982) 317.
[34] D. S. KOLTUN, Adv. Nucl. Phys. *3* (1969) 71.
[35] T. I. KOPALEISHVILI, Particles and Nuclei 2/2 (1971) 87.
[36] J. HÜFNER, Phys. Rep. *21* (1975) 1.
[37] H. K. WALTER, Proc. 7th Int. Conf. on High Energy Physics and Nuclear Structure, Zürich (1977) 225; H. K. WALTER, Conf. on Clustering Aspects of Nuclear Structure and Nuclear Reactions, Winnipeg (1978), A.I.P. Conference Proceedings No. 47 (1978) 444.
[38] N. STANTON, Chicago Operations Office Report COO-1545-92 (1971).
[39] R. A. CECIL, B. D. ANDERSON and R. MADEY, Nucl. Instr. and Meth. *161* (1979) 439.
[40] A. DEL GUERRA, Nucl. Instr. and Meth. *135* (1976) 337.
[41] P. VERNIN, SACLAY, private communication (1978).
[42] M. DROSG, Nucl. Instr. and Meth. *105* (1972) 573.
[43] J. L. FOWLER, J. A. COOKSON, M. HUSSAIN, R. B. SCHWARTZ, M. T. SWINHOE, C. WISE and C. A. UTTLEY, Nucl. Instr. and Meth. *175* (1980) 449.
[44] R. A. J. RIDDLE, G. H. HARRISON, P. G. ROOS and M. J. SALTMARSH, Nucl. Instr. and Meth. *121* (1974) 445.
[45] M. W. MCNAUGHTON, F. BRADY, W. B. BROSTE, A. L. SAGLE and S. W. JOHNSON, Nucl. Instr. and Meth. *116* (1974) 25.
[46] M. ANGHINOLFI, G. RICCO, P. CORVISIERO and F. MASULLI, Nucl. Instr. and Meth. *165* (1979) 217.